Fault intersection and induced seismicity: the effects on the induced stress field and the dynamic rupture, and their implications

Jingming Ruan, Ranajit Ghose, Delft University of Technology; Wim Mulder, Shell Global Solutions International B.V. & Delft University of Technology*

SUMMARY

Intersecting faults are often ignored in the geomechanical simulation of induced seismicity. To investigate the effects of fault intersection and the resulting reservoir geometry on induced seismicity, caused, for instance, by gas extraction, we have developed 3D geomechanical models considering two intersecting normal faults and the surrounding horst structure. We simulate the stress field and the dynamic fault reactivation in a uniformly depleted reservoir. We observe that a smaller intersection angle increases the incremental Coulomb stress at the lower reservoir juxtaposition, thus changing the temporal rupture pattern of the seismic event. In our dynamic simulation, the rupture propagates from the main fault to the secondary fault. We conclude that the fault intersection has important effects on the induced seismicity and should be taken into account when evaluating the seismicity risk in a specific region.

INTRODUCTION

Human activities related to fluid extraction and injection in an underground reservoir induce stress perturbations. The altered stress field can reactivate pre-existing faults in the region. For instance, gas production in the Groningen gas field, the Netherlands, causes numerous induced earthquakes. The poroelastic stress from a uniformly depleted reservoir has been modeled extensively in earlier numerical studies. The results show that the stress concentration caused by the fault offset changes the depletion value required to cause a seismic event as well as the rupture pattern.

However, faults are usually part of a fault system. They separate the reservoir into multiple compartments, depending on the fault offset at the reservoir, and form complicated structures, including horst and graben. Such structures have not been investigated for their role in induced seismicity. They can be studied through 3D geomechanical simulation of intersecting faults. An example is the Zeerijp 2018 M_L 3.4 event that occurred in a region close to the intersection of two faults (Dost et al., 2020).

The seismic rupture from a main fault can propagate to a secondary fault through an intersection. It is difficult to derive the truncation relationship, which depends on the slip at both faults. Therefore, we should consider the fault intersection during the simulation of induced seismic rupture.

To that end, we design 3D geomechanical models to investigate the effects of fault intersection and the resulting reservoir geometry on the induced seismicity, focusing on the angle of the intersection. We simulate both stress field and the fault reactivation, considering mechanically intersecting faults. We validate our findings on realistic models based on the Zeerijp region of the Groningen gas field and the Zeerijp 2018 M_L3.4 event.

GEOMECHANICAL SIMULATION AND THE FAULT CONSTRAINT

We use the open-source package Defmod (Meng, 2017) to simulate the stress field, due to long-term gas extraction, and the fault reactivation during the seismic event. We simulate the induced stress field in a uniformly depleted reservoir. During this stage, the model is considered stable, and the stress equilibrium is estimated at every depletion step using the governing equations:

$$\mathbf{K}_n\mathbf{U}_n = \mathbf{F}_n \text{ (absolute)}, \quad \mathbf{K}_n\Delta\mathbf{U}_n = \Delta\mathbf{F}_n \text{ (incremental)}, \tag{1}$$

where $\mathbf{K}$ is the system stiffness matrix, $\mathbf{U}$ is the solution vector and $\mathbf{F}$ the nodal force, including fluid source. The subscript n is the time index. The solution $\Delta\mathbf{U}_n$ includes the nodal displacement and the pressure: $\Delta\mathbf{U}_n = \begin{bmatrix} \Delta\mathbf{u}_n \\ \Delta\mathbf{p}_n \end{bmatrix}$.

The stiffness matrix $\mathbf{K}_n$ and the right-hand-side vector $\mathbf{F}_n$ have the following form:

$$\mathbf{K}_n = \begin{bmatrix} \mathbf{K}_e & \mathbf{H} \\ -\mathbf{H}^T & \Delta t\mathbf{K}_c + \mathbf{S}_p \end{bmatrix}, \ \Delta\mathbf{F}_n = \begin{bmatrix} \Delta\mathbf{f}_n \\ \mathbf{q}_n - \Delta t\mathbf{K}_c\mathbf{p}_{n-1} \end{bmatrix}, \tag{2}$$

where $\mathbf{K}_e$ is the elastic stiffness matrix, which depends on the elastic constants of the solid. $\mathbf{K}_c$ is the fluid stiffness matrix, which is governed by the fluid-flow conductivity. $\mathbf{H}$ is the coupling matrix and depends on the Biot coefficient, which is responsible for coupling the displacement to the pressure fields. The storage matrix, $\mathbf{S}_p$, depends on solid and fluid compressibility as well as porosity. The combination of the system is accomplished by the coupling matrix $\mathbf{H}$. The solution of the system provides the equilibrium between the displacement and pressure fields.

As the stress field at a pre-existing fault becomes critical, i.e., the shear stress exceeds the fault strength, we simulate dynamically the fault reactivation and the wavefield generated by the seismic rupture using the elastodynamic equations:

$$\mathbf{M}\ddot{\mathbf{u}} + \mathbf{C}\dot{\mathbf{u}} + \mathbf{K}\mathbf{u} = \mathbf{f}, \tag{3}$$

where $\mathbf{M}$ is the mass matrix, $\mathbf{C} = \alpha_\eta\mathbf{M} + \beta_\eta\mathbf{K}$ is the damping matrix, and α and β are the Rayleigh damping coefficients. `Defmod` implements the fault constraint with split nodes and the Lagrange multiplier method. For the constraint implementation on the fault intersection, the crosslink constraint approach is used. For details on the implementation of fault constraint, see Meng (2017) and Meng and Hager (2020).

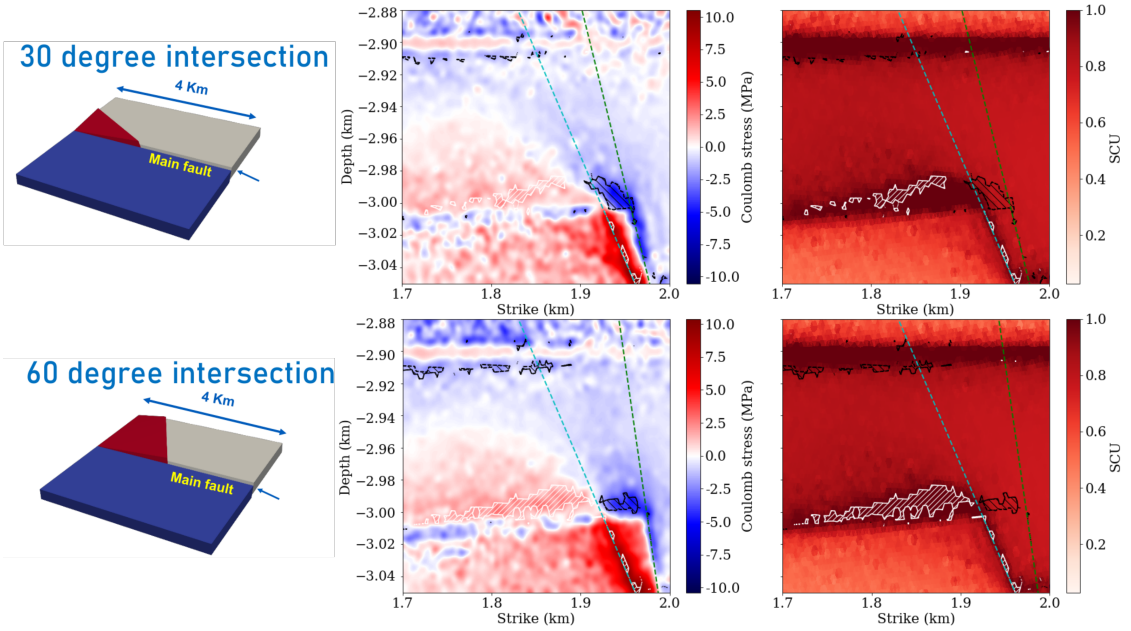

Figure 1: Intersecting fault geometry in the simplified models, and the comparison of incremental Coulomb stress and SCU along the main fault for different intersection angles. Top: the difference between 30° and 45° intersection. Bottom: the difference between 30° and 60° intersection. Taken from Ruan et al. (2023). The white dashed area in the SCU value indicates the increased area of initial slip patch in the model with 30° intersection.

SIMPLIFIED MODELS

To investigate the effects of fault intersection and the resulting reservoir geometry, we design a set of simplified models based on the actual reservoir geometry in the Zeerijp region, to simulate induced seismicity at a uniformly depleted reservoir. We perform 3D geomechanical simulation considering the reservoir geometry created by two intersecting normal faults. By changing the intersection angle, we change the shape of the horst structures. We investigate the difference in the induced stress field and the resulting dynamic rupture. To focus on the effects of the intersecting faults, the material properties are considered to be homogeneous inside the model.

Through changing the intersection angle between two normal faults, we develop models representing 30°, 45°, and 60° intersections. We initiate the model with gravity and gravity-based boundary traction. To achieve this, we load a model having a conventional fault intersection, as it is stable without opening up the intersection during the initial loading. After the initial loading, the crosslink constraint at the intersection is used for simulating the depletion as well as the dynamic rupture when the fault is reactivated. From the initial loading, the stress field at the fault is calculated. Both faults are stable at this stage. Then, we uniformly deplete the reservoir in the quasi-static simulation. We evaluate the stress field at the faults until they become critical. Thereafter, we dynamically simulate the fault reactivation. During the rupture propagation, the event could be aseismic or seismic.

Figure 1 shows the shear capacity utilization *SCU*, which is the ratio between the shear stress and the maximum friction, for models with 30° and 60° fault intersection angle, after 12 MPa depletion of the reservoir. The shear capacity utilization *SCU* show a clear offset-controlled incremental stress field, identical to the pattern for only one fault in a 2D scenario observed by Buijze et al. (2019) and Jansen and Meulenbroek (2022). The latter derived an analytical expression for the induced stress due to a uniformly depleted reservoir. Apart from this common feature with the single-fault model, the effect of the intersecting faults on the incremental stress is primarily focused on the reservoir juxtaposition close to the intersection. Figure 1 also shows the difference in incremental Coulomb stress at both faults between the models with 30° and 60° intersection angles, after 12 MPa reservoir depletion. Note that the intersection angle affects the location of the reservoir compartment, thus also strongly affecting the distribution of the pressure depletion on both faults. The lower half of the reservoir juxtaposition shows a positive value, indicating the promotion of slip in this part. The maximum value is observed at the fault intersection below the reservoir juxtaposition, which results in the slip of the secondary fault, despite low incremental and initial stress at a vertical fault.

Figure 2 shows the results of dynamic simulation for a simplified model with a 45° fault intersection. The depletion value required to trigger an earthquake is similar for different representative models of the intersection angle. Its value is around 12.6 MPa. As mentioned earlier, the change in the Coulomb stress, for models with different fault intersections, causes a shift of the location of the initial slip patch and the location of the maximum slip.

Our results show that the rupture can propagate from the main

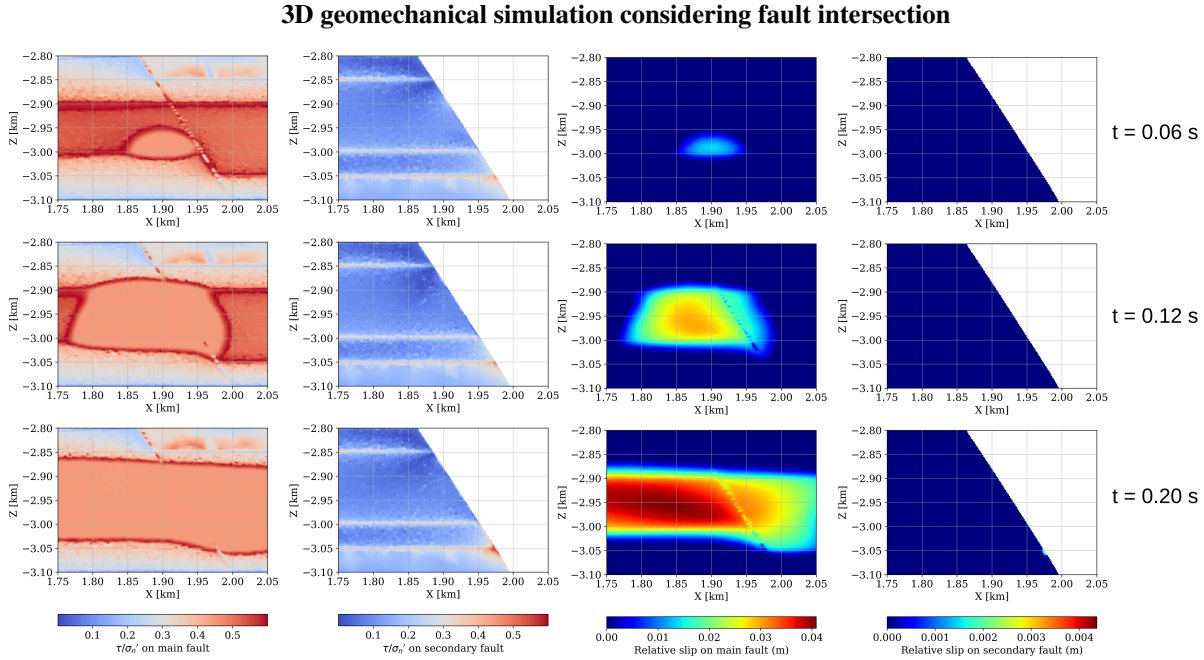

Figure 2: The seismic rupture at both faults for the model with a 45° fault-intersection angle after 12.6 MPa depletion within the reservoir. Left: the ratio between the shear stress and effective normal stress. Right: relative slip.

fault to the secondary fault through the intersection. However, the rupture at the secondary fault is only limited to the lower boundary of the reservoir near the intersection.

The compaction of the triangular horst structure introduces not only vertical compaction but also horizontal compaction. What is different from a single-fault model is that the horizontal compaction through the offset of the reservoir at both faults together increases the effective normal stress at the top of the horst structure at the fault intersection, and decreases below the horst structure at the intersection, which contributes to the confined slip at the secondary fault.

The main fault accommodates most of the rupture during the seismic event in all models. With different intersection angles, the pattern of rupture propagation during the seismic event changes. The 30° intersection shows an initial slip patch located at the lower reservoir juxtaposition close to the intersection. It propagates upward till the upper boundary of the juxtaposition and laterally within the juxtaposition. The 60° intersection shows an initial slip patch located at the lower juxtaposition close to the intersection and propagates upward laterally within the juxtaposition. The locations of the maximum slip for models with 30° and 60° intersections are identical to the initial slip patch. The 45° intersection shows an intermediate pattern, compared to the other two models, with the initial slip patch located at the top of the juxtaposition and the maximum slip at the lower juxtaposition.

The slip at the secondary fault is triggered by the rupture at the main fault when the rupture propagation reaches the intersection at the lower juxtaposition. As mentioned above, the slip at the secondary fault is limited to the intersection below the juxtaposition in all models. The slip patches are similar in both size and amplitude.

ZEERIJP MODEL

To validate our findings on an actual field-scale reservoir geometry, we constructed the Zeerijp model from a Petrel geological model of the Groningen gas field (NAM, 2020). The model comprises several formations, including overburden, top seal, reservoir, and underburden. The material properties are taken from Wentinck (2018) and were estimated from seismic data. Figure 3 shows the reservoir geometry of the Zeerijp model. The intersection angle between the two faults is about 44.5°.

We follow the same approach as described above for initializing the model subject to gravity. Uniform depletion is assumed in the reservoir. After 26 MPa depletion in the reservoir, the Zeerijp model has a seismic event of magnitude $M_L = 3.0$, with parameters similar to the 2018 Zeerijp earthquake of $M_L 3.4$, as reported by Wentinck (2018). Figure 3 shows the fault slip at both faults after the seismic event. Similar to the 45° intersection model, the rupture initiates from the upper slip patch at the main fault and then propagates downward and laterally within the reservoir juxtaposition. The slip at the secondary fault is also triggered when the slip of the main fault reaches the intersection at the lower juxtaposition. The maximum slip is located at the center of the juxtaposition on the main fault. The location of the rupture is close to the location of the inverted hypocenter of the 2018 earthquake by Dost et al. (2020).

CONCLUSION

By quasi-static and dynamic simulations of induced seismicity, taking into account intersecting faults and the resulting horst structure, we studied how the intersection angle between two

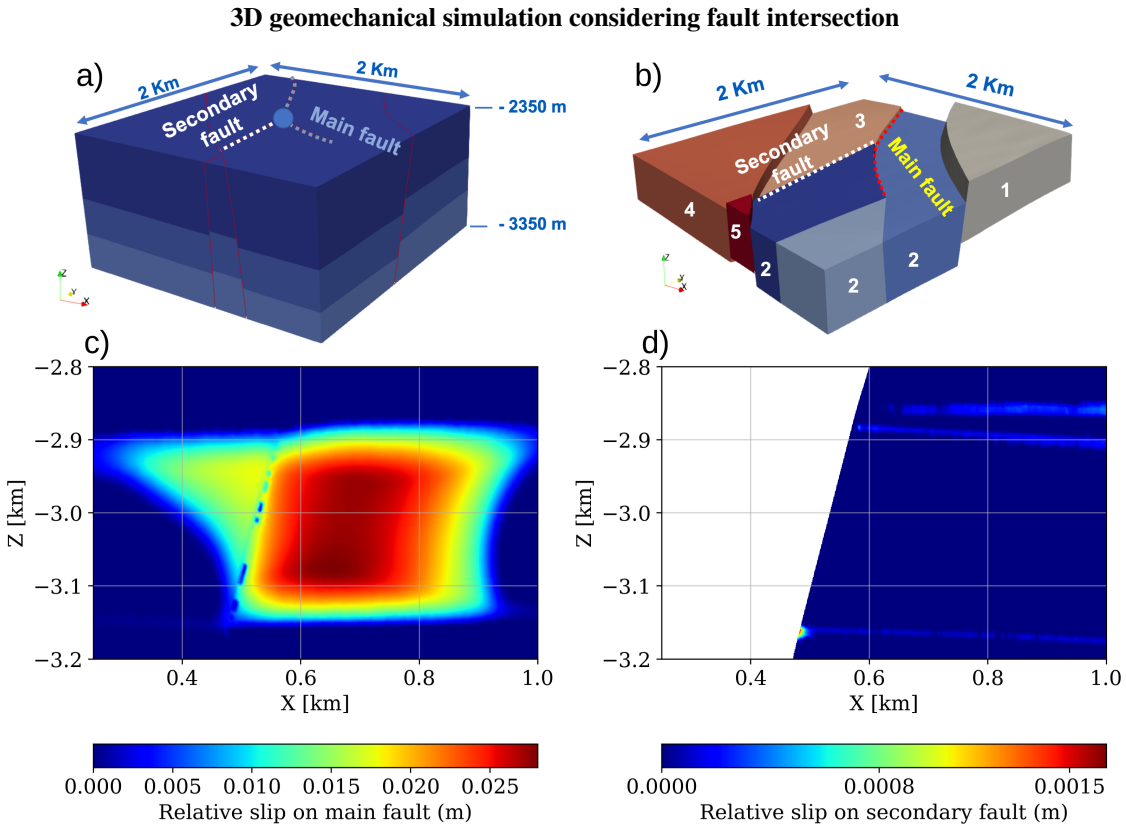

Figure 3: a) Geometry of the Zeerijp model. b) The reservoir geometry of the Zeerijp model. c-d) Dynamic fault slip at both faults in the Zeerijp model after 26 MPa uniform depletion within the reservoir.

faults affects the stress field and the seismic rupture. The compaction of the intersecting flanks of the horst structure at the top (base) of the structure introduces an increase (decrease) of the effective normal stress at the same location. Furthermore, a smaller intersection angle increases the incremental Coulomb stress at the lower reservoir juxtaposition, therefore changing the pattern of the rupture propagation from the upper juxtaposition to the lower one. The secondary fault, which has less incremental shear stress in case of a 90° fault dip, is therefore triggered by the slip at the main fault through the intersection. However, the slip at the secondary fault is limited at the intersection close to the base of the horst structure.

Our simulation, using a realistic reservoir geometry in the Zeerijp region, shows a rupture pattern which is similar to the simplified model. The results from the seismic event resemble those of the inversion of the 2018 Zeerijp M_L3.4 earthquake.

ACKNOWLEDGMENTS

This research was funded by NWO Science domain (NWO-ENW), project **DEEP.NL.2018.048**. We thank Chunfang Meng for providing technical support on Defmod.

REFERENCES

Buijze, L., P. Van den Bogert, B. Wassing, and B. Orlic, 2019, Nucleation and arrest of dynamic rupture induced by reservoir depletion: Journal of Geophysical Research: Solid Earth, **124**, 3620–3645, doi: https://doi.org/10.1029/2018JB016941.

Dost, B., A. van Stiphout, D. Kühn, M. Kortekaas, E. Ruigrok, and S. Heimann, 2020, Probabilistic moment tensor inversion for hydrocarbon-induced seismicity in the Groningen gas field, the Netherlands, part 2: Application: Bulletin of the Seismological Society of America, **110**, 2112–2123, doi: https://doi.org/10.1785/0120200076.

Jansen, J.-D., and B. Meulenbroek, 2022, Induced aseismic slip and the onset of seismicity in displaced faults: Netherlands Journal of Geosciences, **101**, doi: https://doi.org/10.1017/njg.2022.9.

Meng, C., 2017, Benchmarking Defmod, an open source FEM code for modeling episodic fault rupture: Computers & Geosciences, **100**, 10–26, doi: https://doi.org/10.1016/j.cageo.2016.11.014.

Meng, C., and B. Hager, 2020, A crosslink constraint method for modeling episodic dynamic rupture on intersecting faults: Seismological Research Letters, **91**, 1030–1041, doi: https://doi.org/10.1785/0220190234.

NAM, 2020, Petrel geological model of the Groningen gas field, the Netherlands.

Ruan, J., R. Ghose, and W. Mulder, 2023, 3D geomechanical modelling of induced seismicity including intersecting faults and reservoir compartments: 84th EAGE Annual Conference & Exhibition, Extended Abstracts, 1–5, doi: https://doi.org/10.3997/2214-4609.202310538.

Wentinck, H., 2018, Dynamic modelling of large tremors in the Groningen field using extended seismic sources: Nederlandse Aardolie Maatschappij BV.